

***p*-type δ -doping quantum wells and superlattices in Si: Self-consistent hole potentials and band structures**

A. L. Rosa, L. M. R. Scolfaro,* R. Enderlein, G. M. Sipahi,[†] and J. R. Leite

Instituto de Física da Universidade de São Paulo, Caixa Postal 66318, 05315-970 São Paulo, SP, Brazil

(Received 8 April 1998)

The hole-subband and -miniband structures of periodically acceptor δ -doped quantum wells and superlattices (SL's) in silicon are calculated self-consistently within the effective-mass theory and the local-density approximation. The full six-band Luttinger-Kohn effective-mass equations are solved, together with Poisson equation, in a plane-wave representation. Nonparabolicities due to couplings between heavy, light, and spin-orbit split bands are fully taken into consideration. To account for exchange and correlation (XC) effects within the multicomponent hole gas, a parametrized expression for the XC potential energy is adopted. Hole band structures, Fermi levels, and potentials are presented for a series of *p*-type δ -doping SL's, varying the acceptor doping concentrations, periods, and doping spreads. The inclusion of the spin-orbit split band is reflected essentially in nonparabolicities, and it starts to play an important role already for intermediate concentrations. For acceptor doping concentrations above $1.1 \times 10^{14} \text{ cm}^{-2}$, the split-off band is populated for SL periods in both SL and isolated well regimes. A comparison with the available experimental data shows fairly good agreement. Particularly, the data reported on admittance and infrared spectroscopies can be reasonably interpreted if one assumes indirect transitions between subbands, as is the case in *p*-type δ -doped GaAs.

[S0163-1829(98)00747-4]

I. INTRODUCTION

δ -doping of semiconductor materials is a powerful tool for creating confined carrier gases of high concentrations and mobilities.¹⁻³ Due to their importance for device applications, most of the δ -doping studies have been carried out on GaAs and Si. In Si, *p*-type δ -doping has been achieved with layer concentrations up to 10^{14} cm^{-2} (Refs. 4-16) and layer widths down to 12 Å.¹⁶ Various methods have been applied to investigate the hole gas of these layers experimentally, such as, for example, transport measurements,⁷⁻¹¹ infrared spectroscopy,¹²⁻¹⁴ photoluminescence studies,¹⁵ and admittance spectroscopy.¹⁶ Confinement effects of holes due to the ionized acceptor wells have clearly been demonstrated in these measurements. Moreover, experimental data have been obtained on the energy spectra of the confined holes.

Much less work has been done, however, on the theoretical understanding of *p*-type δ -doping wells in Si. While the energy band structures of *n*-type¹⁷⁻²⁷ and *p*-type²⁸⁻³⁴ δ -doping wells in GaAs and those of *n*-type δ -doping wells in Si (Refs. 35-37) are well known from self-consistent envelope-function calculations using realistic bulk band structures, no such calculations exist for *p*-type δ -doping wells in Si. So far, these wells have been studied only by means of one-band effective-mass calculations,^{13,14,16,38-40} in which couplings between different hole bands due to the δ -doping perturbation potential is omitted. Moreover, band nonparabolicities were neglected and anisotropies were either considered in an approximate way^{13,14,16,38} or omitted entirely.^{39,40} The spin-orbit split band was taken into account in Ref. 14 and left out in Refs. 13,16, and 38-40. The uncoupled effective-mass equations were self-consistently solved with regard to exchange-correlation effects^{13,14,38} or without.^{16,39,40}

Results based on the above simplifications cannot be expected to be quantitatively correct, as has been demonstrated

in the calculations for *p*-type δ -doping systems in GaAs.^{32,33} In Si, these simplifications are expected to be even less reliable than in GaAs. Indeed, in Si, the coupling between heavy- and light-hole bands is more important than in GaAs because the splitting between heavy- and light-hole subbands is very small, owing to the fact that the masses of the two types of holes in the [001] direction (the normal direction of the δ -doping planes) are very close to each other (0.29 and 0.20 for heavy and light holes, respectively⁴¹). Moreover, band anisotropies are stronger because the Luttinger parameters γ_3 , γ_2 have a larger difference in Si ($\gamma_3 - \gamma_2 = 1.44 - 0.39$) than in GaAs ($\gamma_3 - \gamma_2 = 2.9 - 2.1$). Finally, band nonparabolicities due to the repulsion of the Γ_8^+ heavy- and light-hole band by the spin-orbit split Γ_7^+ band are already important for energies as small as 44 meV, the spin-orbit splitting energy Δ of Si.⁴¹ As the binding energies E_B of holes in Si *p*-type δ -doping wells are expected to be in the range of 100 meV, the spin-orbit split band must be included. If Δ was even smaller compared to E_B , the spinless Γ_{25}' description of the valence band would be sufficient. But in Si this is not the case. This material forms an "intermediate" case which requires that, first, spin and spin-orbit interactions are taken into account, transforming the spinless Γ_{25}' band into the Γ_8 and Γ_7 bands, and second, that besides the Γ_8 band, also the Γ_7 band is considered. The latter will manifest itself in two different ways. First, as has already been mentioned, it results in essential nonparabolicities in energy regions where the confined states are formed. Hence, an effect on Γ_8 -derived confined states exists even if Γ_7 -derived confined states are not occupied by holes. Second, as we will see below, for sheet doping concentrations above $1.1 \times 10^{14} \text{ cm}^{-2}$, the Γ_7 -derived confined hole states are partially occupied, i.e., additional states occur in the occupied part of the energy eigenvalue spectrum. Simultaneously, these states affect all other states because they change the self-consistent potential.

The need to consider the Γ_7 band implies that the full six-band Luttinger-Kohn (LK) model must be used in a consistent theory of p -type δ -doping structures in Si, unlike p -type δ -doping structures in GaAs for which only the four-band LK model based on the Γ_8 suffices.^{28–34} A general method for solving the four-band LK effective-mass equation for p -type δ -doping structures has been developed in Ref. 32. The method relies on the supercell concept, which means considering a superlattice (SL) of δ -doping layers rather than an isolated layer. The isolated layer case is obtained by making the SL period d sufficiently large. The SL periodicity of the system allows one to represent the effective-mass equation with respect to plane waves of discrete wave vectors. In Sec. II of the present paper, this method is generalized in order to solve the six-band LK effective-mass equation for p -type δ -doping structures. Since exchange-correlation effects are expected to be as important as in GaAs,^{32–34} these effects have to be taken into account in an appropriate way. This is accomplished by generalizing the procedure developed for GaAs in Ref. 32 to the case of Si. In Sec. III, the generalized method is used to calculate self-consistent potentials, subband and miniband structures, as well as Fermi-level positions for a series of p -type δ -doping quantum wells in Si. To compare with experimental results, the doping layers are taken as (100) planes and the doping concentrations are varied between $1 \times 10^{12} \text{ cm}^{-2}$ and $2 \times 10^{14} \text{ cm}^{-2}$. The spread of the doping layers is also varied to investigate its effect on the hole band structures. These studies are mainly performed on large period SL's corresponding to isolated wells,⁴² to which most of the experimental results refer. A few short period SL's with coupled wells are treated for comparison. The calculated potential wells and band structures are compared with previous theoretical and available experimental results.

The paper is organized as follows. In Sec. II we present the calculation method. Section III is devoted to the presentation and discussion of the results. Section IV summarizes our conclusions.

II. METHOD

A. Effective-mass equation

The one-particle Hamiltonian H of the interacting hole gas of a p -type δ -doping SL may be written as

$$H = H_0 + V(\mathbf{x}), \quad (1)$$

where H_0 means the one-particle Hamiltonian of the unperturbed bulk crystal and $V(\mathbf{x})$ the perturbation potential induced by p -type δ -doping. The hole eigenstates $\psi_\lambda(\mathbf{x}, s)$ and eigenenergies E_λ of the SL are determined by the one-particle Schrödinger equation

$$[H_0 + V(\mathbf{x})]\psi_\lambda(\mathbf{x}, s) = E_\lambda \psi_\lambda(\mathbf{x}, s). \quad (2)$$

We assume an infinite extension of the SL in all directions, which allows us to apply periodic boundary conditions for the solutions $\psi_\lambda(\mathbf{x}, s)$ of Eq. (2). With an even number of Si-Si bilayers per SL unit cell, the corresponding periodicity region may be taken as tetragonal with side length $G_z d$ parallel to the [001] SL axis (which is taken to be the z axis of our Cartesian-coordinate system), and side length $G_\parallel (a/\sqrt{2})$ in the two perpendicular directions [110] and $[1\bar{1}0]$; here G_z and G_\parallel are large integers and a is the host lattice constant.

In effective-mass theory, the one-electron Schrödinger equation (2) is represented with respect to the Bloch states $(\mathbf{x}s|\lambda\mathbf{k})$ of first order $\mathbf{k} \cdot \vec{\pi}$ perturbation theory.^{43,44} The eigenstates $\psi_\lambda(\mathbf{x}, s)$ considered here are composed of Γ_8 valence-band states $(\mathbf{x}s|\frac{3}{2}m_{3/2}\mathbf{k})$, $m_{3/2} = \pm\frac{3}{2}, \pm\frac{1}{2}$ and Γ_7 valence-band states $(\mathbf{x}s|\frac{1}{2}m_{1/2}\mathbf{k})$, $m_{1/2} = \pm\frac{1}{2}$. Thus we may write

$$\psi_\lambda(\mathbf{x}, s) = \sum_{jm_j} F_{jm_j}^\lambda(\mathbf{k})(\mathbf{x}s|jm_j\mathbf{k}), \quad (3)$$

where $F_{jm_j}^\lambda(\mathbf{k}) \equiv (jm_j\mathbf{k}|\psi_\lambda)$ are the components of $\psi_\lambda(\mathbf{x}, s)$ with respect to the approximate Bloch states $(\mathbf{x}s|jm_j\mathbf{k})$, known as envelope functions. They obey the effective-mass equations

$$\sum_{j'm'_j\mathbf{k}'} [\delta_{\mathbf{k}\mathbf{k}'}(jm_j\mathbf{k}|H|j'm'_j\mathbf{k}') + (jm_j\mathbf{k}|V|j'm'_j\mathbf{k}')] F_{j'm'_j}^\lambda(\mathbf{k}') = \epsilon_\lambda F_{jm_j}^\lambda(\mathbf{k}). \quad (4)$$

The 6×6 matrix $(jm_j\mathbf{k}|H|j'm'_j\mathbf{k}')$ is given by^{43,44}

$$\begin{array}{cccccc} Q & S & R & 0 & \frac{i}{\sqrt{2}}S & -i\sqrt{2}R \\ S^* & T & 0 & R & -\frac{i}{\sqrt{2}}(Q-T) & i\sqrt{\frac{3}{2}}S \\ R^* & 0 & T & -S & -i\sqrt{\frac{3}{2}}S^* & -\frac{i}{\sqrt{2}}(Q-T) \\ 0 & R^* & -S^* & Q & -i\sqrt{2}R^* & -\frac{i}{\sqrt{2}}S^* \\ -\frac{i}{\sqrt{2}}S^* & \frac{i}{\sqrt{2}}(Q-T) & i\sqrt{\frac{3}{2}}S & i\sqrt{2}R & \frac{1}{2}(Q+T)-\Delta & 0 \\ i\sqrt{2}R^* & -i\sqrt{\frac{3}{2}}S^* & -\frac{i}{\sqrt{2}}(Q-T) & \frac{i}{\sqrt{2}}S & 0 & \frac{1}{2}(Q+T)-\Delta \end{array}, \quad (5)$$

where rows and columns are ordered in sequence $j = \frac{3}{2}, m_{3/2} = \frac{3}{2}, \dots, j = \frac{1}{2}, m_{1/2} = -\frac{1}{2}$, and Q, S, R, T are defined as

$$Q = -\frac{\hbar^2}{2m} [(\gamma_1 + \gamma_2)(k_x^2 + k_y^2) + (\gamma_1 - 2\gamma_2)k_z^2], \quad (6)$$

$$T = -\frac{\hbar^2}{2m} [(\gamma_1 - \gamma_2)(k_x^2 + k_y^2) + (\gamma_1 + 2\gamma_2)k_z^2], \quad (7)$$

$$S = i\frac{\hbar^2}{m}\sqrt{3}\gamma_3(k_x - ik_y)k_z, \quad (8)$$

$$R = -\frac{\hbar^2}{2m}\sqrt{3}[\gamma_2(k_x^2 - k_y^2) - 2i\gamma_3k_xk_z]. \quad (9)$$

The potential term of the effective-mass equation is composed of the Coulomb potential $V_A(\mathbf{x})$ of the ionized acceptor atoms, added to the Hartree potential $V_H(\mathbf{x})$, and the exchange-correlation $V_{XC}(\mathbf{x})$ of the interacting hole gas. The distribution of the ionized dopant atoms along the SL axis is approximated by a Gaussian, centered at the nominal δ -doping layers. Parallel to the layers, the dopant charge is homogeneously smeared out (for a justification of this approximation, see Ref. 37). Thus, the ionized dopant distribution $N_A(z)$ depends only on z and is given by the expression

$$N_A(z) = N_A \sum_{n=-\infty}^{\infty} \frac{1}{\sqrt{2\pi\sigma}} e^{-(z-nd)^2/2\sigma^2}, \quad (10)$$

where N_A means the sheet acceptor doping concentration of a dopant layer and σ^2 is the variance of the Gaussian distribution. The square root of the variance, σ , represents the mean distance of a doping atom from the nominal doping plane. For the full width Δz at half maximum of the Gaussian, one has $\Delta z = 2\sqrt{2 \ln 2} \sigma = 2.355 \sigma$. Because of the form (10) of $N_A(z)$, the ionized acceptor potential is a function $V_A(z)$ of z only. The Hartree and exchange-correlation potentials also depend only on z because their fluctuating parts which depend on x, y , are omitted in the effective-mass approximation. Using the abbreviation

$$V_C(z) = V_A(z) + V_H(z) \quad (11)$$

for the total Coulomb potential, the total perturbation potential $V(\mathbf{x})$ may be written as

$$V(\mathbf{x}) \equiv V(z) = V_C(z) + V_{XC}(z). \quad (12)$$

Because of the independence of the perturbation potential $V(\mathbf{x})$ of the position vector component \mathbf{x}_{\parallel} parallel to the layers and because of the SL periodicity of $V(z)$, the envelope function $F_{jm_j}^{\nu\mathbf{q}}(\mathbf{x})$ in coordinate space may be written as the product of a plane wave having a wave vector \mathbf{q}_{\parallel} parallel to the layers and a z -dependent Bloch function of the SL having a certain quasi-wave-vector q_z of the first SL Brillouin zone and a certain SL band index ν . Thus, setting $\lambda = \nu\mathbf{q}$, the envelope functions $F_{jm_j}^{\nu\mathbf{q}}(\mathbf{k})$ in \mathbf{k} space may be written as

$$F_{jm_j}^{\nu\mathbf{q}}(\mathbf{k}) = \delta_{\mathbf{k}\mathbf{q} + K\mathbf{e}_z} F_{jm_j}^{\nu\mathbf{q}}(K), \quad (13)$$

where K means a vector of the reciprocal SL and \mathbf{e}_z is a unit vector in the z direction. The Fourier coefficients $F_{jm_j}^{\nu\mathbf{q}}(K)$ of the SL Bloch function are determined by the effective-mass equation (4). One obtains

$$\begin{aligned} & \sum_{j'm'_j} \sum_{K'} [\delta_{KK'}(jm_j\mathbf{q} + K\mathbf{e}_z | H | j'm'_j\mathbf{q} + K'\mathbf{e}_z) \\ & + (jm_j\mathbf{q} + K\mathbf{e}_z | V | j'm'_j\mathbf{q} + K'\mathbf{e}_z)] F_{j'm'_j}^{\nu\mathbf{q}}(K') \\ & = E_{\nu\mathbf{q}} F_{jm_j}^{\nu\mathbf{q}}(K). \end{aligned} \quad (14)$$

B. Coulomb potential

Within effective-mass theory, the off-diagonal elements of the Coulomb potential matrix $(jm_j\mathbf{q} + K\mathbf{e}_z | V_C | j'm'_j\mathbf{q} + K'\mathbf{e}_z)$ with respect to $jm_j, j'm'_j$ are neglected, hence

$$(jm_j\mathbf{q} + K\mathbf{e}_z | V_C | j'm'_j\mathbf{q} + K'\mathbf{e}_z) = \delta_{jj'} \delta_{m_j m'_j} (K | V_C | K'), \quad (15)$$

with $(K | V_C | K') \equiv (K - K' | V_C)$ as Fourier coefficients of $V(z)$. The latter obey Poisson's equation

$$(K | V_C | K') = -\frac{4\pi e^2}{\epsilon} \frac{1}{|K - K'|^2} [K | p(z) - N_A(z) | K'] \quad (16)$$

with

$$p(z) = \sum_{\nu\mathbf{q}} \sum_s \frac{1}{\Omega_0} \int_{\Omega_0} d^3\mathbf{x} |\psi_{\nu\mathbf{q}}(\mathbf{x}, s)|^2 \left[1 - \frac{1}{e^{[E_{\nu\mathbf{q}} - E_F]/kT} + 1} \right] \quad (17)$$

being the hole concentration averaged with respect to a bulk unit cell of volume Ω_0 , ϵ the static dielectric constant, and E_F the Fermi energy. Charge neutrality ensures that $[K | p(z) - N_A(z) | K] = 0$. The true SL eigenfunctions $\psi_{\nu\mathbf{q}}(\mathbf{x}, s)$ follow by means of Eqs. (3) and (13). One has approximately

$$\psi_{\nu\mathbf{q}}(\mathbf{x}, s) = \frac{1}{\sqrt{\Omega_0}} e^{i(\mathbf{q} + K\mathbf{e}_z) \cdot \mathbf{x}} \sum_{jm_j} \sum_K F_{jm_j}^{\nu\mathbf{q}}(K) (\mathbf{x}s | jm_j \mathbf{0}), \quad (18)$$

where the Bloch factors of the bulk Bloch functions $(\mathbf{x}s | jm_j \mathbf{k})$ in Eq. (3) have been replaced by the Bloch factors $(\mathbf{x}s | jm_j \mathbf{0})$ at $\mathbf{k} = \mathbf{0}$. Evaluating expression (17) for $p(z)$ by means of Eq. (18) yields

$$\begin{aligned} p(z) &= \frac{1}{\Omega_0} \sum_{\nu\mathbf{q}} \sum_{KK'} \sum_{jm_j} e^{i(K-K')z} F_{jm_j}^{\nu\mathbf{q}*}(K') F_{jm_j}^{\nu\mathbf{q}}(K) \\ &\times \left[1 - \frac{1}{e^{[E_{\nu\mathbf{q}} - E_F]/kT} + 1} \right]. \end{aligned} \quad (19)$$

C. Exchange-correlation potential

The exchange-correlation potential matrix $(jm_j\mathbf{k} | V_{XC} | j'm'_j\mathbf{k}')$ has off-diagonal elements both with respect to $jm_j, j'm'_j$, and K, K' . Neglecting any exchange-

correlation induced couplings between the three different types of carriers involved, i.e., heavy and light holes and spin-orbit-split holes, the (6×6) exchange-correlation matrix of the LK model decomposes into the (4×4) block for heavy and light holes and the (2×2) block for spin-orbit-split holes. For the latter, the (2×2) exchange-correlation potential matrix is diagonal with respect to $m_{1/2}, m'_{1/2}$. In the local-density approximation (LDA), the diagonal elements may be obtained by means of the exchange-correlation potential of a homogeneous electron gas. Parametrized expressions for the latter have been proposed by various authors. We use the expression given by Hedin and Lundqvist.⁴⁵ Screening the electron-electron interaction potential by means of the static dielectric constant of Si, and replacing the free-electron mass and density by, respectively, the effective mass m_{so} and density $p_{so}(z)$ of the spin-orbit split holes, one obtains

$$V_{XC}^{so}(z) = -\frac{e^2}{2\epsilon a_B^{so}} \left(\frac{2}{\pi \alpha r_s(z)} \right) - \frac{e^2}{2\epsilon a_B^{so}} \left(\frac{2}{\pi \alpha} \right) 0.0368 \ln \left(1 + \frac{21}{r_s(z)} \right), \quad (20)$$

where $a_B^{so} = \epsilon(m_0/m_{so})a_B$ is the effective Bohr radius, $\alpha = (4/9\pi)^{1/3}$ is a numerical constant, and $r_s(z) = [(4\pi/3)a_B^{so} p_{so}(z)]^{-1/3}$ is the dimensionless screening radius.

Expression (20) cannot directly be applied to the heavy- and light-hole gas of the Γ_8 valence band. How one may proceed in this case has been shown in our previous work³² where the exchange-correlation potential matrix has been derived for the (4×4) LK model. It has the general form

$$\left(\frac{3}{2} m_{3/2} \mathbf{k} | V_{XC} | \frac{3}{2} m'_{3/2} \mathbf{k}' \right) = \begin{pmatrix} Q_{XC}(\mathbf{k}, \mathbf{k}') & S_{XC}(\mathbf{k}, \mathbf{k}') & R_{XC}(\mathbf{k}, \mathbf{k}') & 0 \\ S_{XC}^*(\mathbf{k}, \mathbf{k}') & T_{XC}(\mathbf{k}, \mathbf{k}') & 0 & R_{XC}(\mathbf{k}, \mathbf{k}') \\ R_{XC}^*(\mathbf{k}, \mathbf{k}') & 0 & T_{XC}(\mathbf{k}, \mathbf{k}') & -S_{XC}(\mathbf{k}, \mathbf{k}') \\ 0 & R_{XC}^*(\mathbf{k}, \mathbf{k}') & -S_{XC}^*(\mathbf{k}, \mathbf{k}') & Q_{XC}(\mathbf{k}, \mathbf{k}') \end{pmatrix}, \quad (21)$$

where the matrix elements are expressions in terms of the exchange-correlation potentials $V_{XC}^{hh}(z)$ and $V_{XC}^{lh}(z)$ of heavy and light holes, respectively. The actual form of these expressions has been given in Refs. 32 and 33, assuming that band warping does not affect the exchange-correlation interaction considerably. The heavy- and light-hole exchange-correlation potentials $V_{XC}^{hh}(z)$ and $V_{XC}^{lh}(z)$ themselves are defined in an analogous way as the exchange-correlation potential $V_{XC}^{so}(z)$ for spin-orbit split holes in Eq. (20). Thereby, the spin-orbit split mass m_{so} is replaced by the isotropic heavy- and light-hole masses \bar{m}_{hh} and \bar{m}_{lh} (we take the experimental values of Ref. 41), and the local bulk spin-orbit-split hole density $p_{so}(z)$ is substituted by the local bulk densities $p_{hh}(z)$ and $p_{lh}(z)$ of heavy and light holes, respectively.

The three partial hole densities need to be known in order to apply the exchange-correlation matrix specified above. To determine these densities in a rigorous way, the SL envelope eigenfunctions $F_{jm_j}^{vq}(\mathbf{k})$ have to be projected onto the various hole eigenstates, and the squared moduli of the components have to be summed up upon all occupied SL bands.⁴⁶ Here we use an approximate procedure. We calculate the total hole density $p(z)$ by means of the SL eigenfunctions, as in the context of Poisson's equation above. The distribution of holes upon the three hole states is obtained by the Thomas-Fermi approximation, i.e., by introducing a local chemical potential $\mu(z)$. In a parabolic approximation one has

$$p_{qh}(z) = \frac{1}{3\pi^2} \left(\frac{2\bar{m}_{qh}}{\hbar^2} \right)^{3/2} \mu(z)^{3/2}, \quad q = h, l, \quad (22)$$

$$p_{so}(z) = \frac{1}{3\pi^2} \left(\frac{2m_{so}}{\hbar^2} \right)^{3/2} \mu(z)^{3/2} \theta(\mu(z) - \Delta), \quad (23)$$

where θ is the Heaviside step function. The chemical potential $\mu(z)$ is determined by the total hole density

$$p(z) = p_{hh}(z) + p_{lh}(z) + p_{so}(z). \quad (24)$$

If $\mu(z) < \Delta$ or, equivalently, if $p(z) < p_t$ with

$$p_t = \frac{1}{3\pi^2} \left(\frac{2}{\hbar^2} \right)^{3/2} (\bar{m}_{hh}^{3/2} + \bar{m}_{lh}^{3/2}) \Delta^{3/2} \quad (25)$$

defined as the threshold density at which the spin-orbit-split band begins to be filled, then $\mu(z)$ is given by the expression

$$\mu(z) = \frac{(3\pi^2)^{2/3}}{2} \hbar^2 (\bar{m}_{hh}^{3/2} + \bar{m}_{lh}^{3/2})^{-2/3} p(z)^{2/3}. \quad (26)$$

For $p(z) > p_t$, no closed analytical solution $\mu(z)$ of Eq. (24) exists anymore. If $p_{so}(z) \ll p(z)$, an approximate solution may be obtained in closed analytical form. It reads

$$\mu(z) = \frac{(3\pi^2)^{2/3}}{2} \hbar^2 (\bar{m}_{hh}^{3/2} + \bar{m}_{lh}^{3/2})^{-2/3} [p(z) - p_{so}^0(z)]^{2/3}, \quad (27)$$

where

$$p_{\text{so}}^0(z) = \frac{1}{3\pi^2} \left(\frac{2m_{\text{so}}}{\hbar^2} \right)^{3/2} \times \left[\frac{(3\pi^2)^{2/3}}{2} \hbar^2 (\bar{m}_{\text{hh}}^{-3/2} + \bar{m}_{\text{lh}}^{-3/2})^{-2/3} p(z)^{2/3} - \Delta \right]^{3/2}. \quad (28)$$

The accuracy of this solution is better than 10% for all densities $p(z)$ above p_t .

D. Bulk properties

The four parameters Δ , γ_1 , γ_2 , and γ_3 of the six-band LK model are crucial for our band-structure calculations of p -type δ -doping SL's in Si. While the spin-orbit splitting energy Δ is well known, $\Delta = 44$ meV,⁴¹ there is a considerable uncertainty with respect to the Luttinger parameters in the literature. The experimental values by Hensel and Feher,⁴⁷ reproduced in Ref. 41, $\gamma_1 = 4.26$, $\gamma_2 = 0.38$, and $\gamma_3 = 1.56$, were our first choice. Self-consistent band-structure calculations for p -type δ -doping SL's employing these values could be carried out without any problems for large SL periods, but, surprisingly, did not converge for small periods. After a long search for the reason for these difficulties, we realized that the choice of the Luttinger parameters was responsible: For small SL periods, wave vectors in [110] become increasingly important. The bulk band structure in this direction, as predicted by the LK model with the Luttinger parameters of Ref. 47, is qualitatively wrong. For energies small compared to Δ , the three bands, i.e., the heavy- and light-hole bands and the spin-orbit split band, bend down, as expected, but, surprisingly, for higher energies compared to Δ , the heavy-hole band starts to bend up. The expression for the heavy-hole mass $m_{\text{hh}}[110]$ in the [110] direction for energies large compared to Δ ,⁴⁴

$$m_{\text{hh}}[110] = \frac{1}{\gamma_1 + \gamma_2 - 3\gamma_3}, \quad (29)$$

reveals the reason for this unphysical behavior. In fact, if the inequality

$$\gamma_1 + \gamma_2 - 3\gamma_3 > 0 \quad (30)$$

is violated, as it happens for the above set of Luttinger parameters ($\gamma_1 + \gamma_2 - 3\gamma_3 = -0.04$), the heavy-hole mass becomes negative and the heavy-hole band must bend up.

Relation (30) imposes a condition on any reasonable set of Luttinger parameters for materials with small spin-orbit splitting energy Δ . For large Δ , this condition may not be applicable because energies large compared to Δ may already lie outside of the range of the LK model. Inspecting the sets of Luttinger parameters from the literature reproduced in Table I, one notices that all other sets^{48–56} fulfill the consistency test (30), although they differ appreciably among each other. We take the set of Ref. 52, $\gamma_1 = 4.22$, $\gamma_2 = 0.39$, and $\gamma_3 = 1.44$. For energies small compared to Δ , this set yields the effective masses shown in Table II. Since, in experiment, the δ -doping layers are (100) planes, the confined states are mainly determined by the [001] masses. In Si, unlike GaAs, these masses are very close to each other for heavy and light holes. This will result in a much smaller

TABLE I. Experimental and theoretical Luttinger parameters of Si from different sources quoted in the text.

	Ref.	γ_1	γ_2	γ_3
Dexter and Lax (1954)	expt. 48	4.00	0.55	1.18
Dresselhaus <i>et al.</i> (1955)	expt. 49	4.00	0.55	1.10
Dexter <i>et al.</i> (1956)	expt. 50	4.00	0.55	1.30
Hensel and Feher (1963)	expt. 47	4.26	0.38	1.56
Balslev and Lawaetz (1965)	expt. 51	4.27	0.32	1.46
Lawaetz (1971)	theor. 52	4.22	0.39	1.44
Chelikowski and Cohen (1974)	theor. 53	4.10	0.44	1.40
Hensel (1982)	expt. 54	4.285	0.339	1.446
Rieger and Vogl (1993)	theor. 55	4.31	0.34	1.43
Persson and Lindefelt (1996)	theor. 56	4.61	0.39	1.54

heavy-hole–light-hole splitting in Si as compared to GaAs. The actual heavy-hole–light-hole splitting in Si is considerably smaller than one expects if the experimental, directionally averaged, isotropic masses of 0.54 and 0.15 are (erroneously) used.

The band structure obtained from the LK model with the Luttinger parameters by Lawaetz⁵² is plotted in Fig. 1 in the three high-symmetry directions [001], [111], and [110]. The dashed lines depict the parabolic approximation. As one can see, nonparabolicities occur already close to Γ , for hole energies of the order of magnitude 10 meV. The nonparabolicities may be characterized as repulsion between the spin-orbit split band and the heavy- and light-hole bands, which pushes the former down and the latter up. The up-shift is negligible for heavy holes in the [001] and [111] directions; in these cases, parabolicity applies over the entire energy range of 200 meV shown in Fig. 1. The fact that the heavy-hole band behaves parabolic in the [001] direction but exhibits nonparabolicities in the [110] direction will affect our band-structure calculations for p -type δ -doping SL's below. We will come back to this point later.

In the estimation of hole concentrations for setting up the exchange-correlation potential, we used an isotropic parabolic approximation of the entire bulk band structure. Although this approximation is too crude to be used in the kinetic energy term of the effective-mass equation, hole energies up to 120 meV are still reproduced fairly well. A Fermi energy of 120 meV corresponds to a total hole density of $p = 10^{20}$ cm⁻³, which puts an upper limit for the isotropic parabolic approximation to be employed in the exchange-correlation potential. Assuming an average hole confinement length of 100 Å, the value $p = 10^{20}$ cm⁻³ is reached for a sheet acceptor doping concentration $N_A = 10^{14}$ cm⁻².

TABLE II. Effective masses of holes in Si for energies small compared to Δ , calculated by means of the Luttinger parameters of Ref. 52. In units of m_0 .

	[100]	[111]	[110]
m_{hh}	0.29	0.75	0.59
m_{lh}	0.20	0.14	0.15
m_{so}	0.24	0.24	0.24

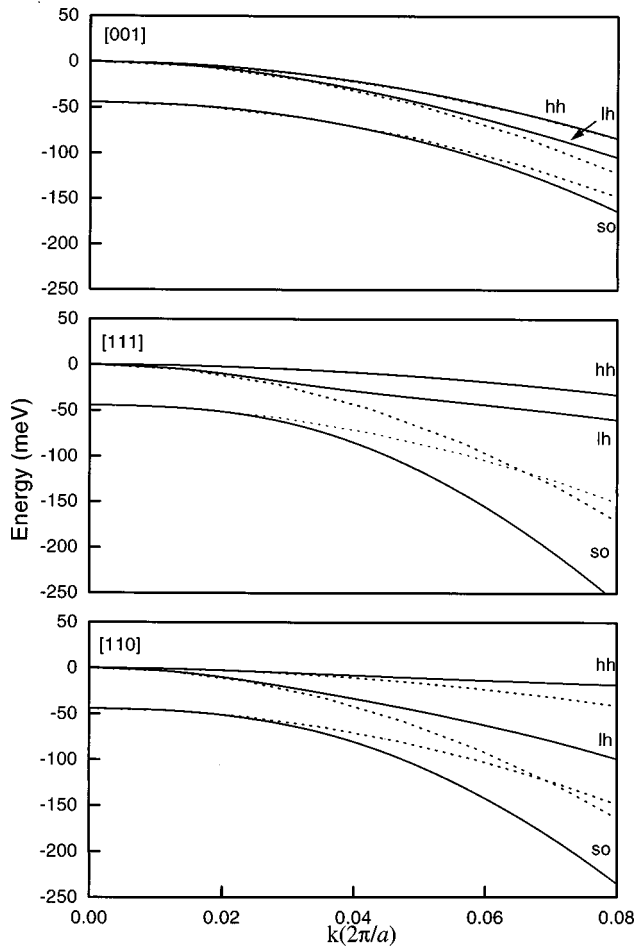


FIG. 1. Valence-band structure of Si calculated within the six-band LK model. The parabolic approximation is shown by dashed lines. Luttinger parameters given in Ref. 52.

III. RESULTS

The results are presented in the next subsections. First, we discuss the characteristic features of self-consistent potentials and band structures of isolated p -type δ -doping wells in Si, taking a particular SL as an example. Then we discuss the changes of potentials and band structures with sheet doping concentration N_A , doping spread Δz , and SL period d . Finally, we compare our results with previous theoretical and experimental findings.

A. General characteristics of isolated p -type δ -doping wells in Si

We consider a SL with a typical sheet doping concentration of $N_A = 5 \times 10^{13} \text{ cm}^{-2}$ and a period of $d = 800 \text{ \AA}$, large enough for the δ -doping wells to be isolated. The doping spread Δz is set equal to 23 \AA . For the static dielectric constant ϵ we used the value 12.1.⁴¹ The self-consistent potential wells and the band structure of this SL are shown in Figs. 2 and 3, respectively. Three different potential wells are depicted in Fig. 2, each corresponding to a particular type of holes, together with the total Coulomb potential well, V_C , due only to the ionized acceptor charge density plus the Hartree contribution. The zeros of the heavy- and light-hole potentials are fixed at the Coulomb potential barriers. These are

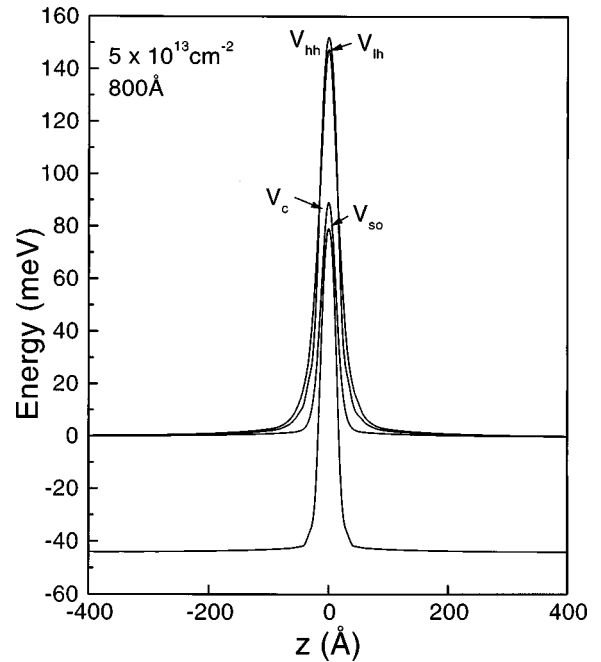


FIG. 2. Self-consistent potential wells of a prototype SL: $N_A = 5 \times 10^{13} \text{ cm}^{-2}$, period of $d = 800 \text{ \AA}$, large enough for the δ -doping wells to be isolated. The doping spread Δz is set equal to 23 \AA .

the same for heavy and light holes, and coincide with the total potential barriers because the exchange-correlation potential parts vanish inside the barriers, due to the vanishing carrier densities there. The barrier for the spin-orbit split holes is shifted down by the spin-orbit splitting energy Δ .

The depths of the wells, V_{hh} , V_{lh} , and V_{so} , amount to 152 meV, 148 meV, and 122 meV for heavy, light and

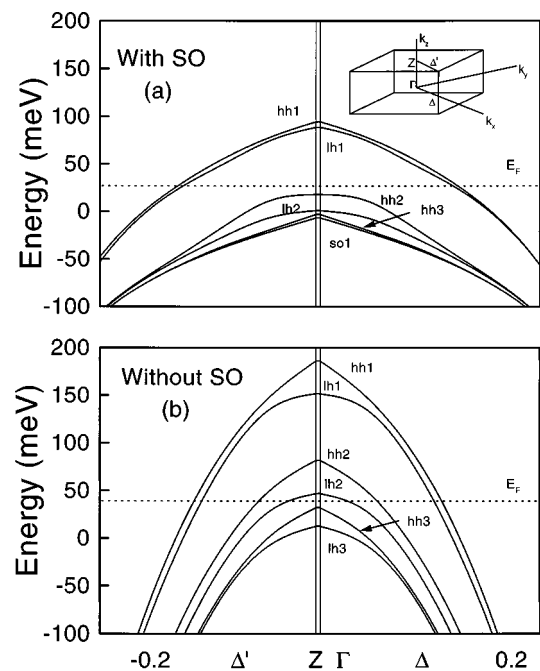


FIG. 3. Band structure of the SL of Fig. 2 along three symmetry lines Γ - Z , Δ , Δ' shown in the inset: (a) with the spin-orbit interaction taken into account and (b) setting the spin-orbit splitting energy Δ to ∞ .

spin-orbit split holes, respectively. The differences are due to the different densities and, consequently, different exchange-correlation potentials for the three types of holes. As no spin-orbit split bands are populated in the SL under consideration, the exchange-correlation potential is zero for the spin-orbit holes, so that the differences $V_{\text{hh}} - V_{\text{so}} = 30$ meV and $V_{\text{lh}} - V_{\text{so}} = 26$ meV represent the exchange-correlation part of the hh and lh hole potentials, respectively.

The heavy- and light-hole wells are shallower for the above p -type δ -doping SL in Si than for an identical doping structure in GaAs, mainly because the occupied light-hole lh1 subband states exhibit stronger confinement in Si than in GaAs. This means stronger screening of the ionized acceptor sheets and shallower potential wells.

The band structure of the SL is plotted in Fig. 3 along the three symmetry lines Γ -Z, Δ , and Δ' of the SL BZ shown in the inset of Fig. 3(a). The bands are labeled as ‘‘hh,’’ ‘‘lh,’’ and ‘‘so’’ according to the bulk states which give the dominant contribution to their formation. Of course, none of these bands is of pure bulk hole type since the bulk hole states are not eigenstates of the SL.

The most characteristic feature of the band structure in Fig. 3(a), which is typical for all p -type δ -doping SL’s in Si, is the distribution of bands into two groups, one group at low energies consisting of the hh1 and lh1 ground-state bands, and a second group of bands at energies close to the barrier and beyond, containing all other bands, among them bands derived from the spin-orbit split bulk band spin orbit. While the hh1-lh1 splitting energy at Γ is only 7 meV, the hh1-hh2 energy splitting at Γ amounts to 75 meV. This reflects, on the one hand, the small difference between the heavy- and light-hole effective masses in the [001] direction, 0.29 and 0.20, in units of the free-electron mass, respectively, and, on the other hand, the relatively *small* values of these masses which give rise to relatively large confinement effects. The hh1-lh1 splitting was even smaller if it was not enlarged by exchange-correlation effects. The latter deepen both subbands, but the hh1 band more than the lh1 band because of the larger density of heavy holes as compared to light holes.

The Fermi level E_F lies between the two band groups, thus only the two ground-state heavy- and light-hole bands are partially populated by holes. In the hh1 band, E_F is 67 meV above the band bottom, and in the lh1 band it is only 60 meV above.

No miniband dispersion along the Γ -Z line occurs, as expected for the large period of 800 Å considered here; one has isolated wells. Solely the highest hh4 miniband has non-zero width. The subband dispersions along Δ , parallel to the SL layers, are more pronounced. It reflects features of the bulk band structure in this plane. Close to Γ , the dispersions of the various subbands differ and exhibit pronounced nonparabolicities. For larger wave vectors on the Δ line, the subbands become parabolic and tend to be parallel to each other. This subband behavior close to and away from Γ is understandable if one realizes that bulk states entering the SL subband states have wave vectors $K\mathbf{e}_z + \mathbf{k}_{\parallel}$, where K is a reciprocal SL lattice vector and \mathbf{k}_{\parallel} denotes the wave-vector component along Δ . Let $|K_0|$ be the range of the dominating SL wave vectors K in the plane expansion of the self-consistent SL potential. Then the relevant bulk wave vectors of an SL subband state of wave vector \mathbf{k}_{\parallel} are $\pm K_0\mathbf{e}_z + \mathbf{k}_{\parallel}$.

With increasing \mathbf{k}_{\parallel} , $\pm K_0\mathbf{e}_z + \mathbf{k}_{\parallel}$ turns over from the cubic [001] direction through [011] into the cubic [010] direction (here we assume Δ along [010]). This implies that the subband nonparabolicities on the Δ line are due to the nonparabolicities of the bulk band along [011], and that the turnover into a parabolic regime at large \mathbf{k}_{\parallel} is due to the parabolicity of the bulk band structure along a cubic direction. As the nonparabolicities of the bulk bands are caused by the repulsion of the heavy- and light-hole bands from the spin-orbit split band, one may also say that the nonparabolicities of the subbands are caused by the spin-orbit split band. The nonparabolicities should decrease if the spin-orbit splitting energy increases. That this in fact happens may be seen from Fig. 3(b), where we plot the band structure of the same SL ($N_A = 5 \times 10^{13}$ cm $^{-2}$ and period 800 Å), but artificially setting the spin-orbit splitting energy Δ to ∞ . The nonparabolicity is reduced although not completely removed. The remaining nonparabolicity is due to the anticrossing of heavy- and light-hole subbands which is well known from GaAs p -type δ -doping SL’s.³²⁻³⁴ In Si p -type δ -doping SL’s, an anticrossing behavior between heavy and light holes also exists for the correct value $\Delta = 44$ meV, but it is smaller and superimposed by effects of the bulk band nonparabolicity due to the spin-orbit split band discussed above.

B. Changes with sheet doping concentration

In Fig. 4, subband structures are compared for SL’s of period 800 Å and three sheet doping concentrations $N_A = 3 \times 10^{12}$ cm $^{-2}$, 3×10^{13} cm $^{-2}$, and 2×10^{14} cm $^{-2}$. For the two lower concentrations, one has two well separated subband groups, the hh1 and lh1 ground-state subbands on one hand, and the group of all higher subbands on the other hand. For the highest concentration, 2×10^{14} cm $^{-2}$, the ground-state spin-orbit split subband so1 has moved out of the second group and stays *between* the two subband groups, well separated from each.

Raising N_A , the subbands become more parabolic. The reason for this transformation is the same as in the nonparabolicity analysis of the preceding subsection: For higher concentrations, the potential wells are steeper and the range $|K_0|$ of reciprocal SL wave vectors K necessary for their plane-wave representation becomes larger. This turns the effective bulk wave vectors $\pm K_0\mathbf{e}_z + \mathbf{k}_{\parallel}$ into the cubic [001] direction where the band structure has only small nonparabolicity.

The variations with doping concentrations of the various subband energy levels at Γ , of the potential well depths V_{hh} , V_{lh} , V_{so} , and of the Fermi energy E_F , are shown in Fig. 5 in more detail. The energy zero is again fixed at the potential barriers. The acceptor concentration N_A was varied from 1×10^{12} cm $^{-2}$ to 2×10^{14} cm $^{-2}$. The well depths increase rapidly with the increase of N_A , reaching about 280 meV for V_{hh} , 260 meV for V_{lh} , and 210 meV for V_{so} at $N_A = 2 \times 10^{14}$ cm $^{-2}$. For the lowest concentration $N_A = 1 \times 10^{12}$ cm $^{-2}$, the potential well depths are about 31 meV for V_{hh} , 26 meV for V_{lh} , and about 16 meV for V_{so} . The ground-state subband levels hh1, lh1, and so1 essentially follow the trend of the well depths. Unlike the former levels, the excited levels hh2, lh2, and hh3 are approximately pinned at the barrier for N_A ranging from 1×10^{12} to 5×10^{13} cm $^{-2}$ with the hh2 and lh2 levels shifting slightly up

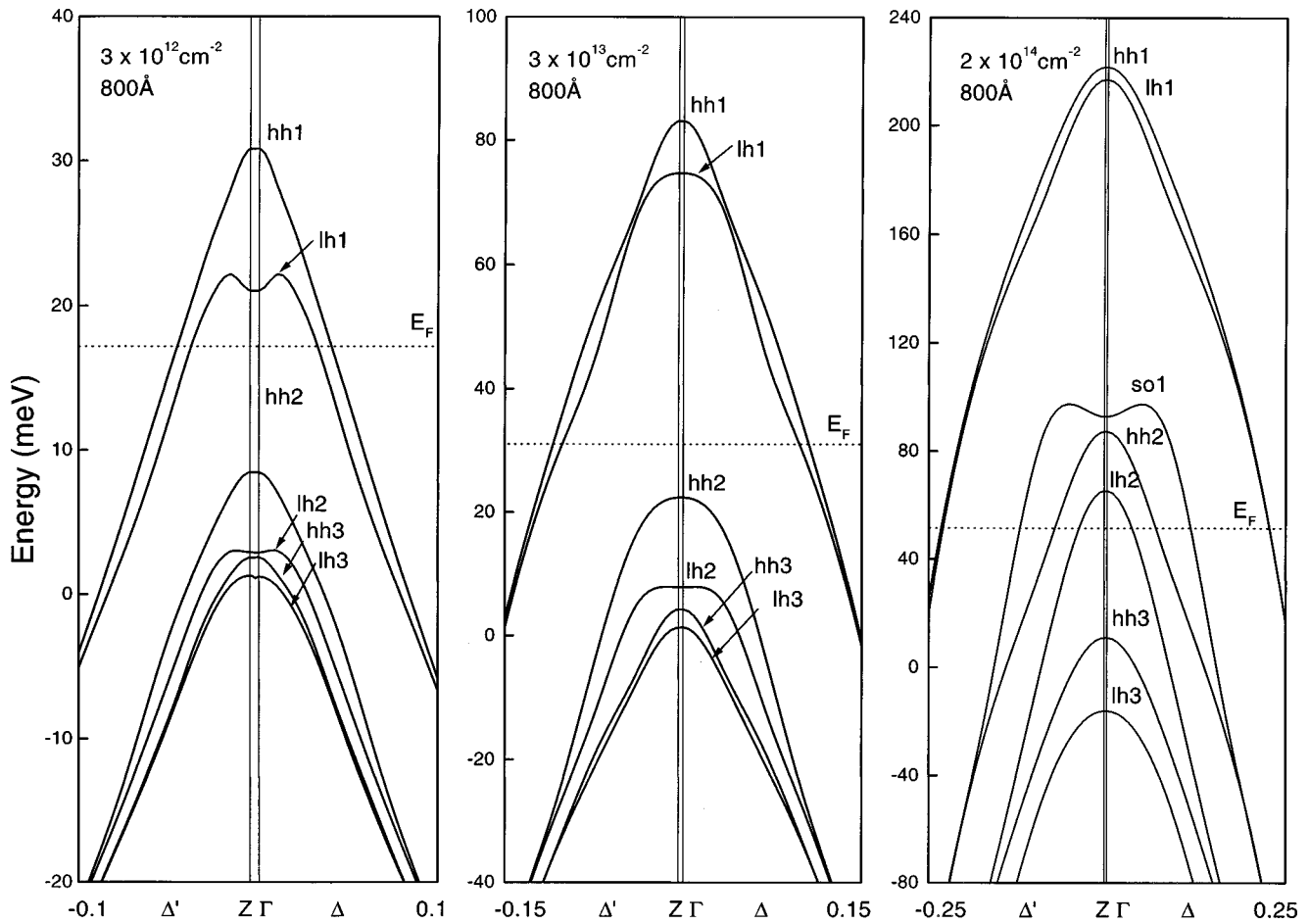


FIG. 4. Band structures for SL's of period 800 Å and three sheet doping concentrations, $N_A = 3 \times 10^{12} \text{ cm}^{-2}$, $3 \times 10^{13} \text{ cm}^{-2}$, and $2 \times 10^{14} \text{ cm}^{-2}$.

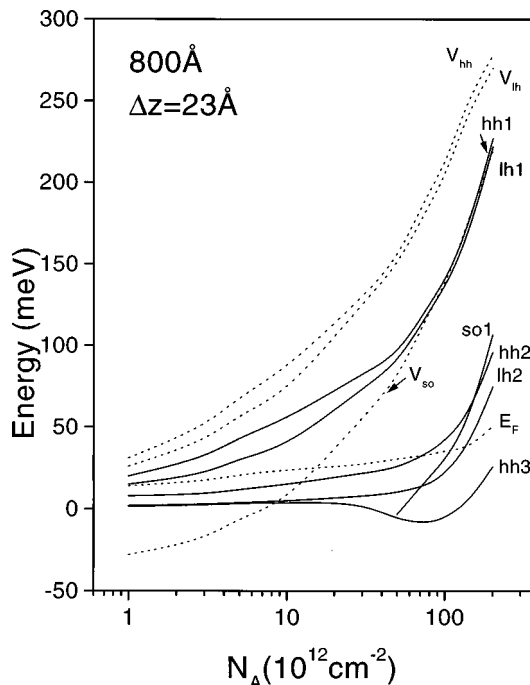


FIG. 5. Variations with doping concentration N_A of the various subband energy levels (solid lines) at Γ , of the potential well depths V_{hh} , V_{lh} , V_{so} , and of the Fermi energy E_F (dashed lines).

while the $hh3$ shifts slightly down. For concentrations above $1 \times 10^{14} \text{ cm}^{-2}$ the excited levels show a steeper increase with the increase of N_A .

The Fermi level E_F also follows the increase of the well depths with raising doping concentrations N_A , however with some delay. The delay results from the increasing band filling with raising N_A . This causes an upshift of E_F which competes with the downshift due to the lowering of all subband levels. It is this competition that, at low concentrations, causes the Fermi level to stay almost constant with respect to the barriers. For concentrations above $8 \times 10^{13} \text{ cm}^{-2}$, higher bands are increasingly populated, thus the available density of states is larger and the Fermi level is almost fixed with respect to the subband bottoms. Their downshifts with increasing N_A are almost completely transferred to E_F . At approximately $1.1 \times 10^{14} \text{ cm}^{-2}$, the Fermi level crosses the $so1$ subband level, meaning that above this concentration the spin-orbit split band is partially populated.

C. Changes with doping spread

It is known from n -type δ -doping SL's in GaAs (Refs. 17–27) and Si (Refs. 35–37) and p -type δ -doping SL's in GaAs (Refs. 28–34) that the width of the δ -doping profiles has an essential effect on the self-consistent potential wells and band structures of such systems. We have performed a systematic study of this effect, taking a SL of period 800 Å

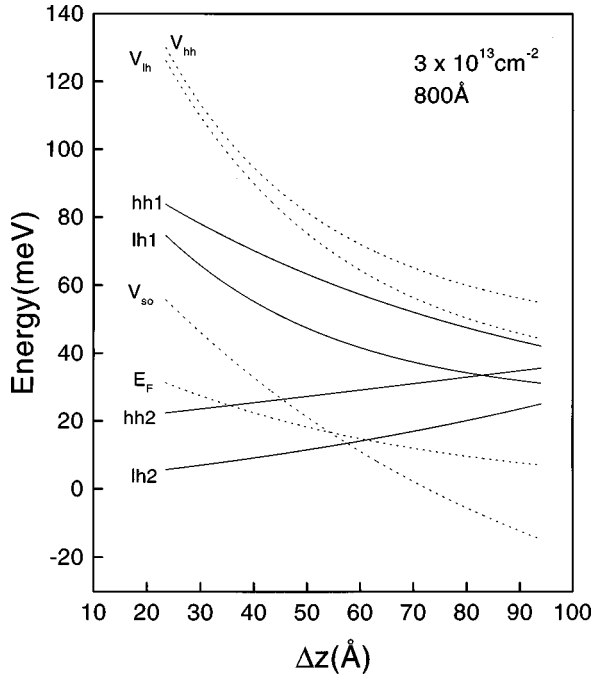


FIG. 6. Potential depths V_{hh} , V_{lh} , V_{so} , the Fermi energy E_F , and the lowest subband levels at Γ as a function of the doping spread Δz .

and sheet doping concentration $N_A = 3 \times 10^{13} \text{ cm}^{-2}$ as an example. The results are depicted in Fig. 6, which shows the potential depths V_{hh} , V_{lh} , and V_{so} , the Fermi energy E_F , and the lowest subband levels at Γ as a function of the doping spread Δz (for a definition of Δz , see Sec. II). Over the entire range of Δz plotted in Fig. 6, the potential wells become flatter. Starting from 130 meV at $\Delta z = 23 \text{ \AA}$, V_{hh} decays down to 65 meV for $\Delta z = 80 \text{ \AA}$. The changes of V_{lh} and V_{so} are comparable. For Δz larger than 80 \AA , one notices a slight deepening of the wells which reflects an interference between neighboring δ -doping layers.

The ground-state subband levels $hh1$ and $lh1$ follow the flattening of the wells, which is plausible because they have their main probability amplitudes there. The two excited $hh2$ and $lh2$ levels shift in the opposite direction because they penetrate into the barriers, which become less effective for the confinement if Δz increases. Strong changes of potential depths and subband levels, as obtained here for a prototype SL, occur for other SL's as well. This means that the doping spread Δz is an important structural parameter of *p*-type δ -doping SL's in Si. It has to be known within 20 \AA , at least, for a comparison between calculated and measured sublevel positions to be reasonable.

D. Changes with SL period

If the SL period decreases, the overlap between hole states localized in different δ -doping wells increases, and a wave-vector dispersion of the minibands starts to develop. This may be seen in Fig. 7, where we plot the band structure of two SL's with a fixed sheet doping concentration $N_A = 1 \times 10^{13} \text{ cm}^{-2}$ and periods $d = 300 \text{ \AA}$ and $d = 100 \text{ \AA}$, respectively. For the 300 \AA SL, a miniband dispersion is observed for the $hh3$ and $lh2$ hole bands and all other bands close to or

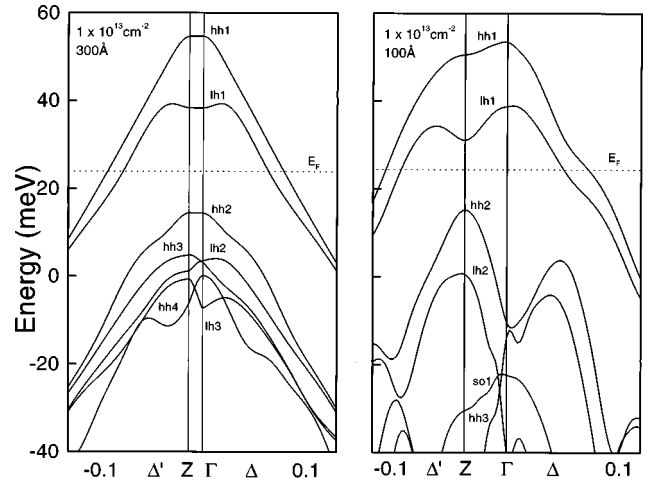


FIG. 7. Band structure of a *p*- δ -doping SL with acceptor doping concentration $N_A = 1 \times 10^{13} \text{ cm}^{-2}$ and periods 300 \AA and 100 \AA .

above the barrier. The three below-barrier minibands $hh1$, $lh1$, and $hh2$ are dispersionless. Considering these latter bands, the SL behaves like a sequence of isolated wells. The hole gas, which populates $hh1$ and $lh1$ bands, is quasi-two-dimensional. For the 100 \AA SL, dispersion is observed for all minibands, including the partially occupied minibands below the Fermi level. The hole gas is no longer two-dimensional but three-dimensional.

Because of their dispersion, some of the minibands cross. As a rule, minibands of different hole types are allowed to cross while minibands of the same hole type show an anticrossing on the Γ - Z line. The subbands on the Δ and Δ' lines may only anticross.

How the miniband dispersion of short-period SL's is influenced by the doping concentration N_A is illustrated in Fig. 8. Shown is the band structure of a SL with $d = 200 \text{ \AA}$ and doping concentration as high as $2 \times 10^{14} \text{ cm}^{-2}$. The potential wells are rather deep in this case and, due to this, none of the below-barrier minibands $hh1$, $lh1$, $so1$, $hh2$, $lh2$, and $hh3$

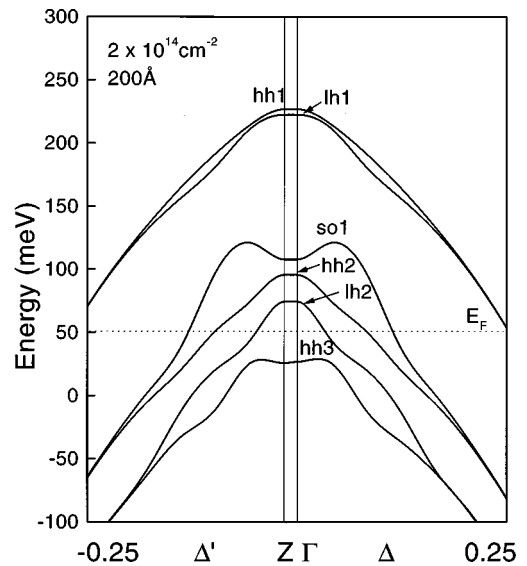


FIG. 8. Band structure of a *p*- δ -doping SL with acceptor concentration $2 \times 10^{14} \text{ cm}^{-2}$ and a period of 200 \AA .

TABLE III. Heavy-hole subband levels at Γ , potential depths, and Fermi-level positions for isolated p -type δ -doping wells in Si with $N_A = 1.4 \times 10^{14} \text{ cm}^{-2}$ and $\Delta z = 35 \text{ \AA}$, calculated by means of a one-band effective-mass equation. The first row shows results extracted from Ref. 38, and the second row displays our results. In the third row, we present results from our approach but with the six-band set of effective-mass equations reduced to a single one-band effective-mass equation (see text for details). The values of the last row have been calculated by adopting the program for n -type δ -doping SL's of Ref. 37 to heavy holes. The zero of energy is fixed at the potential barrier. All energies are given in meV.

V_{hh}	E_F	hh1	hh2	hh3	hh4	hh5	
500		422	259	120	50		Ref. 38
252	37	172	57	4			Present work
400	5	375	335	267	174	60	Simplified
570	5	485	310	152	56	13	Ref. 37

exhibits a dispersion. The δ -potential wells are almost isolated, and the hole gas is quasi-two-dimensional, despite the short period of 200 \AA .

E. Comparison with previous calculations

As has been mentioned before, in all previous calculations^{13,14,16,38-40} various simplifications on the set of six-band effective-mass equations have been made. One-band effective-mass theory has been used, even if heavy, light, and spin-orbit split holes were distinguished. As a consequence, nonparabolicities of bulk bands and any couplings between bulk bands due to the δ -doping potential were left out. Nevertheless, it is interesting to compare the results of these calculations with our results. For comparison, we take a large-period SL with $N_A = 1.4 \times 10^{14} \text{ cm}^{-2}$ and $\Delta z = 35 \text{ \AA}$, whose heavy-hole sublevels at Γ have been calculated in Ref. 38. The results reported in this reference and our own results are compiled in Table III. One notices that the levels of Ref. 38 are much deeper than ours. Similar discrepancies exist between our results and those reported in other papers,^{13,14,16,39,40} in all cases the previously calculated sublevels are much deeper than the ones calculated here.

To check if these discrepancies are actually caused by the simplifications of the effective-mass equations, rather than by other reasons such as, for instance, the use of different sets of expansion functions, we artificially introduce these simplifications into our calculations. Exchange-correlation effects are omitted, as in Ref. 38. The spin-orbit splitting energy Δ is set to ∞ , the Luttinger parameters γ_2 and γ_3 are taken to be equal, γ_1 is set to 500, and $\gamma_2 = \gamma_3$ to 498. This choice yields the same heavy-hole mass ($1/m_{\text{hh}}[001]) = 0.3$ as in Ref. 38. The light-hole mass is extremely small, ($1/m_{\text{lh}}[001]) = 0.001$. This small value ensures that the light-hole levels are very shallow and not populated by holes. The latter fact allows us to compare our simplified calculations with those of Ref. 38, which do not take light holes into account. The results of the simplified calculations are shown in the third row of Table III. The potential well depth V_{hh} is very deep, as in Ref. 38. The differences are probably due to the slightly different heavy-hole masses parallel to the layers; while we assumed 0.3, a value of 0.4 was used in the above-mentioned previous calculations.

TABLE IV. Infrared absorption data extracted from Refs. 14 and 38. We denote the absorption edge at low energy by $P_{<}$, that at high energy by $P_{>}$, and the absorption band maximum by P_{max} . The parameters of the samples are the sheet doping concentration N_A , which is given below, and the spread, $\Delta z = 35 \text{ \AA}$, which is the same for all samples.

N_A (10^{13} cm^{-2})	2.5	5	10	14	20
	Ref. 14	Ref. 38	Ref. 14	Ref. 14	Ref. 14
$P_{<}$ (meV)	130	120	150	200	220
$P_{>}$ (meV)	350	350	400	550	600
P_{max} (meV)	210	205	260	360	390

We also compare the results of our simplified calculations with results which follow by adopting a program developed for n -type δ -doping SL's (Ref. 37) to heavy holes. The results are shown in the last row of Table III. As expected, they are in fairly good agreement with the results of our simplified calculations. In both cases, the Fermi level is close to the barrier, much higher than in the rigorous calculations. The small discrepancies could be due to the fact that while the simplified calculations (performed within the six-band LK model with an appropriate choice of parameters) do indeed minimize the light- and heavy-hole coupling, they do not completely eliminate it.

In conclusion, the discrepancies between the present and previous calculations are in fact due to the simplifications made previously on the effective-mass equations. The main effect of these simplifications is an underestimation of the density of states (DOS) of the lowest subbands. In the rigorous calculations, these bands are much flatter and, consequently, their state densities are much higher than the simplified calculations suggest. The small DOS values of the simplified calculations push the Fermi level considerably up and cause states to be populated by holes which are rather delocalized and ineffective for screening of the ionized acceptor sheets. Thus, the potential wells and all sublevels become deeper than in our calculations. The Fermi level is close to the barriers in the previous calculations, a result which is clearly ruled out by PL measurements (see below).¹⁵

F. Comparison with experiment

We compare our results with experimental data obtained by means of three different methods: infrared absorption spectroscopy, admittance spectroscopy, and photoluminescence spectroscopy.

1. Infrared absorption spectroscopy

Infrared absorption spectra have been measured on a variety of p -type δ -doping SL's.^{12-14,38} The period d was 300 \AA in all cases, and the sheet doping concentration N_A and width Δz of the doping layer were varied. Each spectrum showed one broadband, originating from optical transitions between subband levels occupied by holes as initial states and subband levels empty of holes as final states. We denote the absorption edge at low energy by $P_{<}$, that at high energy by $P_{>}$, and the absorption band maximum by P_{max} . These energies are summarized in Table IV, together with the pa-

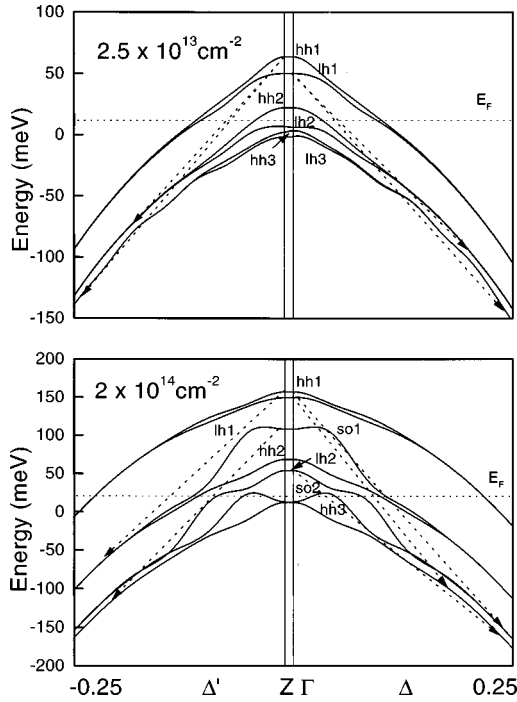


FIG. 9. Calculated band structures of two SL's, with a period of 300 Å, those with the lowest and highest doping concentrations, $2.5 \times 10^{13} \text{ cm}^{-2}$ and $2 \times 10^{14} \text{ cm}^{-2}$, in Table IV are shown in (a) and (b), respectively. Some possible intrasubband transitions are indicated by dashed arrows.

rameters of the samples, N_A and Δz , from which they were measured.

Calculated band structures of two of the SL's, those with the lowest and highest doping concentrations, $2.5 \times 10^{13} \text{ cm}^{-2}$ and $2 \times 10^{14} \text{ cm}^{-2}$, are shown in Figs. 9(a) and 9(b). For the first SL, the hh1, lh1, and hh2 subbands are partially populated; these bands may act as initial states, and all higher bands as final states. For the second SL, the hh1, lh1, so1, hh2, lh2, and so2 subbands are partially filled and are possible as initial states, while all other subbands may function as final states. Ideally, the envelope eigenfunctions of the subbands have defined parity at Γ , thus only transitions between initial bands of even (odd) and final bands of odd (even) parity are symmetry allowed. In reality, the potential well is not ideally symmetric, due to nonzero background and surface charge densities. Thus, all transitions will give nonvanishing contributions, although the strongest transitions should be those between hh1 and hh3, and between lh1 and lh3, due to a larger overlap between the wave functions. The corresponding direct transition energies at Γ are 80 meV and 65 meV for the first SL, and about 200 meV for the second SL. These energies are considerably smaller than the experimental peak positions of 210 meV and 390 meV, respectively. This discrepancy has already been noticed by the authors in Ref. 13, and attributed to many-body corrections such as depolarization and excitonlike effects. However, analyzing the absorption spectra, one has to be aware that the level separation at Γ cannot *a priori* be identified with the position of the absorption peak. Due to the cubic bulk symmetry of Si, all of the intersubband transitions are dipole forbidden at Γ , and their oscillator strength is proportional to the square of the wave-vector component \mathbf{k}_{\parallel}

TABLE V. Experimental activation energies E_{act} from admittance spectroscopy of Ref. 16 and calculated band separation energies ΔE extracted from our band-structure calculations for three p -type δ -doping samples.

N_A (10^{13} cm^{-2})	Δz (Å)	E_{act} (meV)	ΔE (meV)
2.4	12	110	95
6.0	30	300	150
10.0	50	340	250

parallel to the δ -doping layers. The peak position is the weighted average of the transition energies at various \mathbf{k}_{\parallel} rather than the transition energy at Γ . But this does not change the theoretical peak positions considerably since the band separations in Fig. 9 are almost independent of \mathbf{k}_{\parallel} . Owing to the latter fact, the absorption bands should be rather narrow, contrary to what has been observed experimentally.

The above considerations rely on direct optical transitions with conservation of the wave-vector component \mathbf{k}_{\parallel} . There are good reasons, however, to assume that \mathbf{k}_{\parallel} conservation is broken in δ -doping SL's, because of the short-range fluctuations of the impurity potential. In fact, experimental PL spectra from p -type δ -doping SL's in GaAs could only be explained if \mathbf{k}_{\parallel} conservation was released.⁵⁷ If indirect transitions are considered in the infrared spectra of p -type δ -doping SL's in Si, the absorption bands become much broader and their maxima reach much higher energies. This is indicated in Fig. 9; the indirect transitions which could be responsible for the experimental absorption maxima are marked by dashed arrows. Thus, assuming indirect transitions, there are at least no more contradictions between the experimental absorption spectra and the calculated band structures. To make a more detailed comparison possible, absorption spectra have to be calculated. This task will be solved in a forthcoming paper.

2. Admittance spectroscopy

In admittance spectroscopy, activation energies E_{act} for exciting carriers from bound states into mobile states are determined by means of capacity measurements.¹⁶ For p -type δ -doping SL's in Si, such measurements have been performed on three different samples in Ref. 16. The parameters of the samples and the measured values E_{act} are reproduced in Table V. Assuming \mathbf{k}_{\parallel} conserving transitions, E_{act} should be the difference ΔE between the highest occupied hole sublevel and the lowest above-barrier sublevel at Γ . The ΔE values obtained from our calculations are shown in the last column of Table V. While for the sample with the lowest doping concentration ΔE compares fairly well with E_{act} , ΔE is considerably smaller than E_{act} for the two samples with the higher concentrations. This resembles the above discrepancy between experimental infrared absorption peaks and calculated direct band separations. Obviously, indirect transitions are also involved in the activation processes of admittance spectroscopy. The fact that the discrepancy is the smallest for the lowest concentration is also plausible: breaking of \mathbf{k}_{\parallel} conservation is the weakest in this case.

3. Photoluminescence spectroscopy

Experimental PL data on p -type δ -doping SL's in Si are rare in the literature. We are only aware of the work by Buyanova *et al.*¹⁵ The indirect fundamental gap of Si and, consequently, the involvement of phonons of various branches in the radiative transitions, causes many spectral features not related to the Q2D hole gas of the δ -doping wells. Nevertheless, in Ref. 15, the Q2D emission band could be uniquely identified. The width of this band is determined by the position of the Fermi level, ΔE_F , with respect to the bottom of the hh1 subband. For a sample with $N_A = 1 \times 10^{13} \text{ cm}^{-2}$, an experimental value of 25 meV has been estimated,¹⁵ and for $N_A = 5 \times 10^{13} \text{ cm}^{-2}$ we extract $\Delta E_F = 55 \text{ meV}$ from the spectrum shown in Ref. 15. Our band-structure calculations for SL's of the two concentrations, assuming isolated wells and a doping spread $\Delta z = 30 \text{ \AA}$, yield $\Delta E_F = 28 \text{ meV}$ and $\Delta E_F = 58 \text{ meV}$, in good agreement with the experimental values. We consider this comparison to be a crucial test because the Fermi level may be determined from the experimental spectra rather directly, without any underlying assumptions on the type of optical transitions. Such assumptions are necessary to extract the subband levels, as discussed above.

IV. CONCLUSIONS

We have presented hole subband and miniband structures of p -type δ -doped quantum wells and superlattices in silicon calculated self-consistently within a full six-band Luttinger-Kohn model, in which heavy, light, and spin-orbit split hole bands are included. Exchange-correlation effects were taken into account in the framework of the local-density approxi-

mation. Hole band structures, potentials, and Fermi-level positions were studied as functions of the acceptor doping concentrations, superlattice periods, and doping spreads. The subband dispersions show a strong anticrossing behavior, due to the small splitting between heavy- and light-hole levels. The inclusion of the spin-orbit split-off band results in pronounced nonparabolicities whose effects on the heavy- and light-hole-derived states are present even if the split-off band is not populated. These findings reinforce the fact that the full 6×6 Luttinger-Kohn Hamiltonian must be solved in order to provide realistic descriptions of the hole band structures. For acceptor doping concentrations above $1.1 \times 10^{14} \text{ cm}^{-2}$, the spin-orbit split band is occupied. The superlattice regime with interacting δ wells is reached for superlattice periods $\leq 200 \text{ \AA}$, for doping concentrations varying between 10^{12} and 10^{14} cm^{-2} . Exchange-correlation effects, as in p -type δ -doping GaAs, are found to play an important role in the p -type δ -doped quantum wells in Si.

The comparison of our results with the available photoluminescence data on δ -doped Si quantum-well samples shows excellent agreement. As wave-vector nonconserving transitions are likely to occur in δ -doping structures, since direct transitions within the valence band are parity forbidden, the admittance and infrared experiments can be only interpreted by assuming indirect transitions.

ACKNOWLEDGMENTS

The authors would like to thank FAPESP, CAPES, and FINEP (Brazilian funding agencies) for partial financial support.

*Author to whom correspondence should be addressed. Electronic address: scolfaro@macbeth.if.usp.br

†Permanent address: Laboratory of Integrated Systems, Polytechnic School, Universidade de São Paulo, Av. Luciano Gualberto, trav. 3, 158, 05508-900, S.P., Brazil.

¹E. F. Schubert and K. Ploog, Jpn. J. Appl. Phys., Part 2 **24**, L608 (1985).

²H. J. Gossmann and E. F. Schubert, CRC Crit. Rev. Solid State Mater. Sci. **18**, 1 (1993).

³E. F. Schubert, in *Epitaxial Microstructures*, edited by Arthur C. Gossard, Semiconductors and Semimetals Vol. 40 (Academic, New York, 1994), p. 1.

⁴M. G. Dowsett, R. D. Barlow, H. S. Fox, R. A. A. Rubiak, and R. Collins, J. Vac. Sci. Technol. B **10**, 336 (1992).

⁵G. Temple, N. Schwarz, F. Müller, F. Koch, H. P. Zeindl, and I. Eisele, Thin Solid Films **184**, 171 (1990).

⁶N. L. Matthey, M. G. Dowsett, E. H. C. Parker, T. E. Whall, S. Taylor, and J. F. Zhang, Appl. Phys. Lett. **57**, 1648 (1990).

⁷H.-J. Gossmann and F. C. Unterwald, Phys. Rev. B **47**, 12 618 (1993).

⁸H. H. Radamson, M. R. Sardela, O. Nur, M. Willander, B. E. Sernelius, W. X. Ni, and G. V. Hansson, Appl. Phys. Lett. **64**, 1842 (1994).

⁹K. Ismail, M. Arafa, K. L. Saenger, J. O. Chu, and B. S. Meyerson, Appl. Phys. Lett. **66**, 1077 (1995).

¹⁰Y. Kiyota, T. Nakamura, and T. Inada, Appl. Surf. Sci. **82/83**, 400 (1994).

¹¹H. Kujirai, E. Murakami, and S. Kimura, Jpn. J. Appl. Phys., Part 1 **34**, 782 (1995).

¹²J. S. Park, R. P. G. Karunasiri, K. L. Wang, Y. J. Mii, and J. Murray, in *Silicon Molecular Beam Epitaxy*, edited by J. C. Bean, S. Iyer, and K. Wang, MRS Symposia Proceedings No. 220 (Material Research Society, Pittsburgh, 1991), p. 85.

¹³K. L. Wang, R. P. G. Karunasiri, and J. S. Park, Surf. Sci. **267**, 74 (1992).

¹⁴G. Karunasiri, Jpn. J. Appl. Phys., Part 1 **33**, 2401 (1994).

¹⁵I. A. Buyanova, W. M. Chen, A. Henry, W.-X. Ni, G. V. Hansson, and B. Monemar, Phys. Rev. B **53**, 9587 (1996).

¹⁶Jian-hong Zhu, Da-wei Gong, Bo Zhang, Fang Lu, Chi Sheng, Heng-hui Sun, and Xun Wang, Phys. Rev. B **52**, 8959 (1995).

¹⁷A. Zrenner, F. Koch, and K. Ploog, Surf. Sci. **196**, 671 (1988).

¹⁸M. Santos, T. Sajoto, A. Zrenner, and M. Shayegan, Appl. Phys. Lett. **53**, 2504 (1988).

¹⁹L. Ioriatti, Phys. Rev. B **41**, 8340 (1990).

²⁰M. H. Degani, J. Appl. Phys. **70**, 4362 (1991).

²¹C. A. C. Mendonça, F. Plentz, J. B. B. Oliveira, E. A. Meneses, L. M. R. Scolfaro, D. Beliaev, S. M. Shibli, and J. R. Leite, Phys. Rev. B **48**, 12 316 (1993).

²²L. Chico, F. García-Moliner, and V. R. Velasco, Phys. Rev. B **48**, 11 427 (1993).

²³S. M. Shibli, L. M. R. Scolfaro, J. R. Leite, C. A. C. Mendonça, F. Plentz, and E. A. Meneses, Appl. Phys. Lett. **60**, 2895 (1992).

²⁴C. A. C. Mendonça, L. M. R. Scolfaro, J. B. B. Oliveira, F.

- Plentz, F. Mikovic, J. R. Leite, and E. A. Meneses, *Superlattices Microstruct.* **12**, 257 (1992).
- ²⁵R. Enderlein, L. M. R. Solfaro, J. M. V. Martins, and J. R. Leite, *Superlattices Microstruct.* **12**, 175 (1992).
- ²⁶L. M. R. Solfaro, J. R. Leite, C. A. C. Mendonça, D. Beliaev, S. M. Shibli, E. C. F. da Silva, and E. A. Meneses, *Mater. Sci. Forum* **143-147**, 669 (1994).
- ²⁷G.-Q. Hai, N. Studart, and F. M. Peeters, *Phys. Rev. B* **52**, 8363 (1995).
- ²⁸D. Richards, J. Wagner, H. Schneider, G. Hensdorfer, M. Maier, A. Fischer, and K. Ploog, *Phys. Rev. B* **47**, 9629 (1993).
- ²⁹F. A. Reboredo and C. R. Proetto, *Phys. Rev. B* **47**, 4655 (1993).
- ³⁰G. M. Sipahi, R. Enderlein, L. M. R. Solfaro, and J. R. Leite, in *Proceedings of the 22nd International Conference on the Physics of Semiconductors*, edited by D. J. Lockwood (World Scientific, Singapore, 1995), p. 687.
- ³¹L. M. Gaggero-Sager and R. Pérez-Alvarez, *J. Appl. Phys.* **79**, 3351 (1995).
- ³²G. M. Sipahi, R. Enderlein, L. M. R. Solfaro, and J. R. Leite, *Phys. Rev. B* **53**, 9930 (1996).
- ³³G. M. Sipahi, R. Enderlein, L. M. R. Solfaro, and J. R. Leite, in *Proceedings of the 7th International Conference on Shallow-Level Centers in Semiconductors*, edited by C. A. J. Ammerlaan and B. Pajot (World Scientific, Amsterdam, 1997), p. 209.
- ³⁴L. E. Ramos, G. M. Sipahi, L. M. R. Solfaro, R. Enderlein, and J. R. Leite, *Superlattices Microstruct.* **22**, 443 (1997).
- ³⁵H. P. Zeindl, T. Wegehaupt, I. Eisele, H. Oppolzer, H. Reisinger, G. Tempel, and F. Koch, *Appl. Phys. Lett.* **50**, 1164 (1987).
- ³⁶I. Eisele, *Superlattices Microstruct.* **6**, 123 (1989).
- ³⁷L. M. R. Solfaro, D. Beliaev, R. Enderlein, and J. R. Leite, *Phys. Rev. B* **50**, 8699 (1994).
- ³⁸J. S. Park, R. P. G. Karunasiri, Y. J. Mii, and K. L. Wang, *Appl. Phys. Lett.* **58**, 1083 (1991).
- ³⁹L. M. Gaggero-Sager and R. Pérez-Alvarez, *Phys. Status Solidi B* **197**, 105 (1996); *Appl. Phys. Lett.* **70**, 212 (1997).
- ⁴⁰L. M. Gaggero-Sager, M. E. Mora-Ramos, and D. A. Contreras-Solorio, *Phys. Rev. B* **57**, 6286 (1997).
- ⁴¹G. Harbeke, O. Madelung, and U. Rössler, in *Numerical Data and Functional Relationships in Science and Technology*, edited by O. Madelung, Landoldt-Börnstein, New Series, Group III, Vol. 17 (Springer-Verlag, Berlin, 1982).
- ⁴²A. L. Rosa, L. M. R. Solfaro, G. M. Sipahi, R. Enderlein, and J. R. Leite, *Microelectron. Eng.* **43-4**, 489 (1998).
- ⁴³J. M. Luttinger and W. Kohn, *Phys. Rev.* **97**, 869 (1955).
- ⁴⁴R. Enderlein and N. J. M. Horing, *Fundamentals of Semiconductor Physics and Devices* (World Scientific, Singapore, 1996).
- ⁴⁵L. Hedin and J. Lundqvist, *J. Phys. C* **4**, 2064 (1971).
- ⁴⁶R. Enderlein, G. M. Sipahi, L. M. R. Solfaro, and J. R. Leite, *Phys. Rev. Lett.* **79**, 3712 (1997).
- ⁴⁷J. C. Hensel and G. Feher, *Phys. Rev.* **129**, 1041 (1963).
- ⁴⁸R. N. Dexter and B. Lax, *Phys. Rev.* **96**, 223 (1954).
- ⁴⁹G. Dresselhaus, A. F. Kip, and C. Kittel, *Phys. Rev.* **98**, 368 (1955).
- ⁵⁰R. N. Dexter, H. J. Zeiger, and B. Lax, *Phys. Rev.* **101**, 637 (1956).
- ⁵¹I. Balslev and P. Lawaetz, *Phys. Lett.* **19**, 6 (1965).
- ⁵²P. Lawaetz, *Phys. Rev. B* **4**, 3460 (1971).
- ⁵³J. R. Chelikowski and M. L. Cohen, *Phys. Rev. B* **10**, 5095 (1974).
- ⁵⁴J. C. Hensel, quoted in Ref. 41 as a private communication.
- ⁵⁵M. Rieger and P. Vogl, *Phys. Rev. B* **48**, 14 276 (1993).
- ⁵⁶C. Persson and U. Lindelfelt, *Phys. Rev. B* **54**, 10 257 (1996).
- ⁵⁷G. M. Sipahi, R. Enderlein, L. M. R. Solfaro, J. R. Leite, E. C. F. da Silva, and A. Levine, *Phys. Rev. B* **57**, 9168 (1998).